Nanocluster explosions and quasimonoenergetic spectra by homogeneously distributed impurity ions

M. Murakami[1,a)] and M. Tanaka[2]

[1]*Institute of Laser Engineering, Osaka University, Osaka 565-0871, Japan*
[2]*National Institute for Fusion Science, Toki, Gifu 509-5292, Japan*

A plasma expansion into vacuum and the resultant ion acceleration are studied analytically and numerically. The expansion of an initially uniform spherical plasma (consisting of a nanocluster or microdroplet) with radius R_{u0} and electron density n_{u0} is driven by the explosion of hot electrons having an initial temperature T_{e0}. A self-similar solution describes the nonrelativistic expansion of a finite plasma mass with a full account of charge separation effects. Such key features as the energy spectrum, maximum ion energy, and energy transfer efficiency from the electrons to the ions are given by simple analytic formulas as a function of the normalized droplet radius, $\Lambda_u = R_{u0}/\lambda_D$, where $\lambda_D = \sqrt{T_{e0}/4\pi n_{u0}e^2}$ is the Debye length. The solution predicts that impurity ions doped homogeneously in a droplet plasma are accelerated quasimonoenergetically by the electrostatic field generated by the charge separation. The prediction is confirmed by *N*-body particle simulations. The origin of the monoenergetic spectrum is attributed to the spherical geometry. © *2008 American Institute of Physics*. [DOI: 10.1063/1.2965147]

I. INTRODUCTION

In the last decade, ion acceleration due to plasma expansions into vacuum under intense laser irradiation has been studied extensively.[1–25] The energy spectrum and the maximum kinetic energy of the accelerated ions have been controversial in many of these theoretical and experimental results. Energetic ions originating from the periphery of the expanding plasma are crucially affected by the properties of the electron sheath beyond the ion front. Much of the relevant analytical work has been based on the quasineutral assumption. Recently, a rigorous self-similar solution[12] has been found for nonquasineutral two-fluid systems composed of electrons and ions, describing the free expansion of a finite plasma with a full account of charge separation effects. However, the solution is mathematically applicable only to limited cases. In the present paper we extend it to practical problems by showing that it agrees with *N*-body particle simulations conducted under general conditions. Figure 1 leads to such questions as: To what extent can the self-similar solution predict the behavior of a plasma expansion for a uniform nanocluster target, and how precisely can one formulate the maximum ion energy and energy transfer from the electrons to the ions. The initial condition is to be achieved by application of an intense, ultrashort laser pulse on a tiny droplet. Although the resultant heating process is an important issue,[6] its detailed analysis is outside of the scope of the present work.

Generation of monoenergetic ions[15–25] is another issue relevant to laser plasma expansions, because it can lead to medical and energy applications, such as, cancer therapy and fast ignition in inertial confinement fusion, respectively. Except in a few cases,[20–23] most studies on the generation of monoenergetic ions have been based on planar geometry. Last and Jortner,[20] for example, numerically showed that Coulomb explosions composed of different species of ions produce quasimonoenergetic ions. Meanwhile, Ter-Avetisyan *et al.*[21] reported experimental evidences for quasimonoenergetic spectra of accelerated ions when using a water droplet. In the present paper we demonstrate that such a quasimonoenergetic energy spectrum, which is observed in a droplet plasma expansion doped with impurity ions, can be explained by using the simple self-similar solution. The origin of the monoenergetic spectrum is concluded to result from the spherical geometry.

The goal of the present paper is to address the dynamics of a droplet plasma expansion with the help of particle simulations and the self-similar solution, and to demonstrate the generation of quasimonoenergetic ions due to the impurity component. The structure of this paper is as follows. In Sec. II we briefly review the self-similar solution by providing some useful fitting formulae for the detailed numerical results and we propose a comprehensive physical picture underlying the phenomena. In Sec. III we extend the self-similar model to an initially uniform droplet plasma and compare it with particle simulation results. In Sec. IV we show that quasimonoenergetic spectra can be obtained for impurity ions doped in a background plasma with a finite mass. Section V is devoted to a summary.

II. ANALYTICAL MODEL

A. Self-similar solution

Suppose that at $t=0$ the electron component of a finite plasma is rapidly heated to a uniform temperature T_{e0}, and that the subsequent plasma expansion is described by a nonrelativistic model of two charged fluids coupled via a self-consistent electric field. It is assumed that the ions remain

---

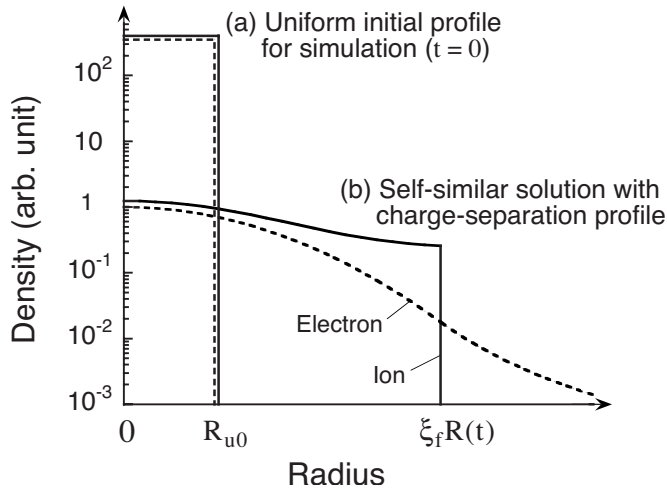a)Electronic mail: murakami-m@ile.osaka-u.ac.jp.

FIG. 1. Initial profiles for (a) the simulation and (b) the self-similar solution, where R_{u0}, ξ_f, and $R(t)$ denote the initial droplet radius, the self-similar coordinate at the ion front, and the characteristic scale in the self-similar system, respectively. The density profiles for the ions and electrons are found to asymptotically approach the self-similar profiles (b).

FIG. 2. Spatial profiles for the normalized ion N_i and electron N_e densities together with the potential Φ and electric field E for $\Lambda_s=1.9$ and $\nu=3$.

cold, whereas the electrons adopt a uniform temperature distribution $T_e(t)$ at each time. This one-dimensional hydrodynamic system is described by[26]

$$\frac{\partial n_{i(e)}}{\partial t} + \frac{1}{r^\nu}\frac{\partial}{\partial r}[r^\nu v_{i(e)} n_{i(e)}] = 0, \tag{1}$$

$$\frac{\partial v_i}{\partial t} + v_i \frac{\partial v_i}{\partial r} + \frac{Ze}{m_i}\frac{\partial \phi}{\partial r} = 0, \tag{2}$$

$$\frac{\partial v_e}{\partial t} + v_e \frac{\partial v_e}{\partial r} + \frac{T_e}{m_e n_e}\frac{\partial n_e}{\partial r} - \frac{e}{m_e}\frac{\partial \phi}{\partial r} = 0, \tag{3}$$

$$\frac{1}{r^\nu}\frac{\partial}{\partial r}\left(r^\nu \frac{\partial \phi}{\partial r}\right) = 4\pi e(n_e - Zn_i), \tag{4}$$

where $\nu = 1$, 2, and 3 correspond, respectively, to planar, cylindrical, and spherical geometries. Equation (1) combines two continuity equations for the electron (subscript e) and ion (subscript i) fluids. The Poisson equation (4) for the electrostatic potential ϕ is written in cgs units; e is the elementary charge and Z is a fixed ionization value.

To find a physically interesting self-similar solution to Eqs. (1)–(4) under the nonquasineutral assumption $n_e \neq Zn_i$, we use the similarity ansatz[30]

$$v_{i(e)}(t,r) = \dot{R}\xi, \quad \xi = \frac{r}{R(t)}, \quad \dot{R} \equiv \frac{dR}{dt}, \tag{5}$$

$$n_e(t,r) = n_{e0}\left(\frac{R_0}{R}\right)^\nu N_e(\xi), \quad N_e(0) = 1, \tag{6}$$

$$Zn_i(t,r) = n_{e0}\left(\frac{R_0}{R}\right)^\nu N_i(\xi), \quad N_i(0) \neq 1, \tag{7}$$

where $n_{e0} \equiv n_e(0,0)$.

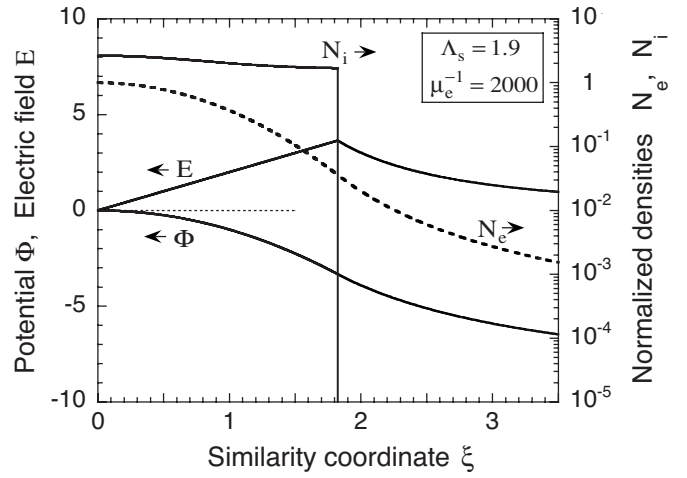In the present system, there are two characteristic scale lengths, the plasma size $R(t)$ and the Debye length

$\lambda_D(t) = \sqrt{T_e(t)/4\pi n_{e0}e^2}$. One can find a self-similar solution if $R(t)$ and $\lambda_D(t)$ evolve coherently in time such that the ratio between them is constant,

$$\Lambda_s = \frac{R}{\lambda_D} = \frac{R_0}{\lambda_{D0}} = R_0\left(\frac{4\pi e^2 n_{e0}}{T_{e0}}\right)^{1/2}, \tag{8}$$

where $R_0 \equiv R(0)$, $\lambda_{D0} \equiv \lambda_D(0)$, and $T_{e0} \equiv T_e(0)$. It should be noted that, within the framework of the self-similar solution, the ion fluid is assumed to have a finite radial extension $0 \leq r \leq \xi_f R$, i.e., a sharp edge at a fixed value ξ_f of the (Lagrangian) self-similar variable ξ [see Fig. 1(b)]. Therefore the functions for the ions, N_i and $v_i/\dot{R}$, are defined only inside the interval $0 \leq \xi \leq \xi_f$, while the electron fluid extends to infinity so that the functions, ϕ, N_e, and $v_e/\dot{R}$, are defined for all $0 \leq \xi < \infty$. The region $\xi_f < \xi < \infty$, where $n_i = 0$, comprises the electron sheath.

Introducing the dimensionless potential,

$$\Phi(\xi) = e\phi/T_e, \tag{9}$$

the present system of Eqs. (1)–(7) yields

$$N_e = \exp(\Phi - \mu_e \xi^2), \quad 0 \leq \xi \leq \infty, \tag{10}$$

where $\mu_e = Zm_e/m_i \ll 1$ is the electron-to-ion mass-overcharge ratio. Here we explain the physical implication of the small but crucial factor μ_e. With Eq. (10), as might be expected,[26] for $\mu_e = 0$ we recover the familiar Boltzmann relation, which is usually employed to close the system of ion fluid Eqs. (1), (2), and (4) without solving them for the electron fluid. The reason why we cannot stay within this conventional approach is as follows. When applying the Boltzmann relation $n_e(t,r) = n_e(t,0)\exp(e\phi/T_e)$ to a dynamic problem, one actually assumes that, at any time t, electrons instantaneously relax to a thermodynamic equilibrium in a given electrostatic potential $\phi = \phi(t,r)$. However, similar to the case of the gravitational field,[27] such an equilibrium, being possible in the planar geometry, does not exist for spherically symmetric finite charge distributions. This is caused by the finite potential difference $\Phi_\infty > -\infty$ between the plasma center and infinity (see Fig. 2 below, for example), which, by
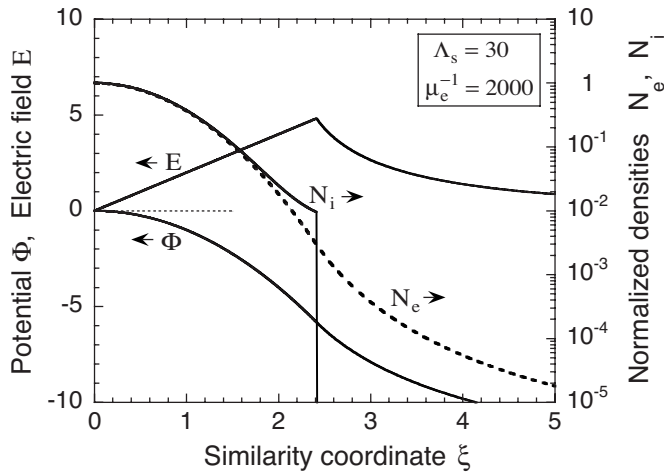
FIG. 3. Spatial profiles for the normalized ion N_i and electron N_e densities together with the potential Φ and electric field E for $\Lambda_s=30$ and $\nu=3$.

virtue of $N_e(\infty)=\exp(\Phi_\infty)>0$ [where $\Phi_\infty \equiv \Phi(\infty)$], implies that the global plasma neutrality can never be ensured with $\mu_e=0$. Consequently, if we choose $\mu_e=0$ (i.e., apply the usual Boltzmann relation), we can solve our problem for $\nu=1$ but not for $\nu=3$. The cylindrical case of $\nu=2$ is less obvious but can be proven to fall in the same category as the spherical one. To overcome this difficulty, we resort to a fully dynamic treatment of the electron fluid with nonzero electron mass ($\mu_e>0$), which leads us to Eq. (10).

In the following, we employ the approximation, $1+\mu_e \simeq 1$. As a result, the profiles in the ion-fluid region $0 \leq \xi \leq \xi_f$ are given by

$$\Phi = -\xi^2, \tag{11}$$

$$E = -d\Phi/d\xi = 2\xi, \tag{12}$$

$$N_e = \exp(-\xi^2), \tag{13}$$

$$N_i = \exp(-\xi^2) + 2\nu \Lambda_s^{-2}, \tag{14}$$

where E in Eq. (12) denotes the normalized electric field.

The ion front ξ_f and the physical profiles for $\xi>\xi_f$ is obtained numerically as an eigenvalue problem.[12] Figures 2 and 3 plot the results for $\Lambda_s=1.9$ and $\Lambda_s=30$, respectively, where $\nu=3$ and $\mu_e^{-1}=2000$ to approximate a proton. As can be seen in Fig. 2, the ion density is rather uniform in space with a strong charge separation. Meanwhile, in Fig. 3 with $\Lambda_s=30$, the ion density profile is closer to a Gaussian shape, and the charge separation can only be observed in the vicinity of the ion front. For both Fig. 2 and Fig. 3, the electric field E linearly increases for $0<\xi<\xi_f$ and asymptotically vanishes as $\xi \to \infty$. In contrast the potential Φ converges to a finite value as $\xi \to \infty$.

B. Energy spectrum and maximum ion energy

The simplest way to evaluate the ion energy spectrum by free plasma expansion would be to ignore the effects of charge separation and solve the appropriate hydrodynamical problem in the quasineutral approximation. In our case, if a spatially uniform electron temperature is assumed, a quasineutral self-similar solution is obtained, giving a Gaussian density profile, $N_e(\xi)=N_i(\xi)=\exp(-\xi^2)$, which extends to infinity. It should be noted that, in the self-similar model,[12] the geometry index ν and the adiabatic index γ cannot be independent of each other, being related by $\gamma=2-2/\nu$; for example, if $\nu=3$ (spherical), then $\gamma=4/3$ is required for the self-consistency of the system. Note that $\gamma=4/3$ is the adiabatic index of the electron gas with $T_e \gg m_e c^2$. However, one may employ an approximation that relaxes this strict condition in order that the model can treat other combinations of ν and γ as follows. The asymptotic ($t \to \infty$) velocity distribution is given by $v_{i(e)}(t,\xi)=v_\infty \xi$, where

$$v_\infty = \lim_{t\to\infty} \dot{R} = \begin{cases} 2c_{s0}/\sqrt{\nu(\gamma-1)}, & \gamma>1, \\ 2c_{s0}\sqrt{\ln(R/R_0)}, & \gamma=1, \end{cases} \tag{15}$$

is obtained by integrating $R\ddot{R}=2c_{s0}^2$,[12] corresponding to the reduced temporal part of the ion momentum equation (2), with the sound speed $c_{s0}=\sqrt{ZT_{e0}/m_i}$ and initial condition $\dot{R}(0)=0$. The first expression for $\gamma>1$ in Eq. (15) applies to a droplet target that is instantaneously heated to temperature T_{e0} by an intense, ultrashort pulse and adiabatically expands after that. On the other hand, if the system expands isothermally under long-pulse irradiation, the first expression in Eq. (15) should be replaced by the second with $\gamma=1$, where v_∞ in this case is roughly estimated at a time when the laser irradiation ceases at $R=R(\tau_p)$ with τ_p the laser pulse duration. The isothermal temperature has the temporal dependence $T_e(t) \propto n_e(t,0)^{\gamma-1} \propto R(t)^{-\nu(\gamma-1)}$, where the mass conservation law $n_e R^\nu = $ constant is used. For spherical adiabatic expansion with $\nu=3$ and $\gamma=5/3$, the system size R evolves as $R(t)/R_0 = \sqrt{1+(2c_{s0}^2/R_0^2)t^2}$ with $\dot{R}(0)=0$ [see Eq. (33) in Ref. 10], and thus $T_e(t) \propto 1/t^2$ at long times, consistent with a kinetic model.[32–34]

The most important output of the self-similar solution is the maximum ion kinetic energy $\mathcal{E}_{i,\max}$ for ions at the vacuum boundary with $\xi=\xi_f$ in the form

$$\mathcal{E}_{i,\max} = \mathcal{E}_0 \xi_f^2, \tag{16}$$

where $\mathcal{E}_0 = \frac{1}{2}m_i v_\infty^2$ is the characteristic energy of an ion at $t \to \infty$ given the two contrasting cases,

$$\mathcal{E}_0 = \begin{cases} 2ZT_{e0}/\nu(\gamma-1), & \gamma>1, \\ 2ZT_{e0}\ln[R(\tau_p)/R_0], & \gamma=1. \end{cases} \tag{17}$$

Again, the conditions $\gamma>1$ and $\gamma=1$ correspond to instantaneous heating ($\tau_p \ll R_0/c_{s0}$) and isothermal expansion due to long laser irradiation ($\tau_p \gg R_0/c_{s0}$), respectively. In the latter case, the plasma expansion is considered to be adiabatic for $t>\tau_p$ after switching off the laser.[10] In spherical geometry, the first expression in Eq. (17) yields a factor of 2 difference between $\mathcal{E}_0=ZT_{e0}$ (Refs. 33 and 34) at $\gamma=5/3$ and $\mathcal{E}_0=2ZT_{e0}$ at $\gamma=4/3$. Since the latter is mathematically self-consistent in our self-similar solution, we keep $\mathcal{E}_0=2ZT_{e0}$ as a reference value when comparing numerical simulations below.
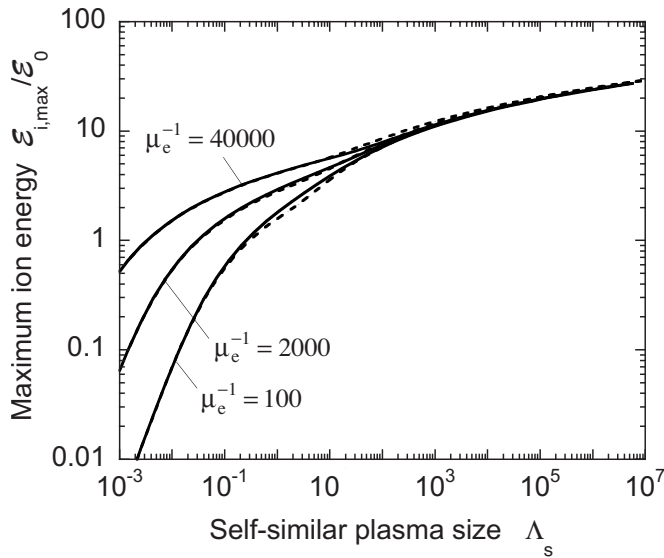
FIG. 4. Maximum ion kinetic energy vs the normalized plasma size for the self-similar solution. The solid and dashed lines represent the detailed numerical results and the fitting formula given by Eqs. (16) and (20), respectively.

FIG. 5. Ion kinetic energy spectra for various values of the self-similar plasma size Λ_s prescribed by Eq. (21). In the limits of $\Lambda_s \to 0$ and $\Lambda \to \infty$, they approach the spectra for a Coulomb explosion of a uniform bare ion sphere and for an ambipolar plasma expansion, respectively.

In spherical geometry ($\nu = 3$), the asymptotic behavior of ξ_f with respect to Λ_s is analytically derived[12] in the limits $\Lambda_s \ll \mu_e^{-1/2}$ and $\Lambda_s \gg \mu_e^{-1/2}$ as follows:

$$\xi_f^2 = \begin{cases} \xi_{fA}^2 = W[\pi^{1/3}\Lambda_s^{4/3}/2\mu_e]/2, & \Lambda_s \ll \mu_e^{-1/2}, \\ \xi_{fB}^2 = W[\Lambda_s^2/2], & \Lambda_s \gg \mu_e^{-1/2}, \end{cases} \quad (18)$$

where the critical value $\Lambda_s \approx \mu_e^{-1/2}$ is obtained from the condition $\xi_{fA} = \xi_{fB}$, and $W(x)$ is the inverse of the function

$$x(W) = W\exp(W), \quad (19)$$

and is called the Lambert W function.[31] Asymptotically, $W(x) \approx x$ for $x \ll 1$ and $W(x) \approx \ln(x/\ln x)$ for $x \gg 1$. Note that the second formula of Eq. (18) for $\Lambda_s \gg \mu_e^{-1/2}$ applies not only to $\nu = 3$ but also to $\nu = 1$ and 2. An approximate value of ξ_f for arbitrary Λ_s is

$$\xi_f \approx (\xi_{fA}^6 + \xi_{fB}^6)^{1/6}, \quad 0 < \Lambda_s < \infty. \quad (20)$$

Figure 4 shows the normalized maximum ion energy $\mathcal{E}_{i,\max}/\mathcal{E}_0$ as a function of Λ_s. The solid curves denote the numerical solutions for different values of μ_e, where $\mu_e^{-1} = 100$ corresponds to a hypothetical light ion, while 2 000 and 40 000 approximately correspond to a proton and a sodium ion, respectively. The dashed curves plot the fitting formula, Eq. (20), and show good agreements with the numerical results. In Fig. 4 the difference in the behavior of ξ_f for the two regimes $\Lambda_s \gg \mu_e^{-1/2}$ and $\Lambda_s \ll \mu_e^{-1/2}$ is attributed to the following: For $\Lambda_s \gg \mu_e^{-1/2}$, the electron sheath extending beyond the ion front $\Delta\xi_f$ becomes much thinner than the ion sphere radius, i.e., $\Delta\xi_f \ll \xi_f$, and therefore the geometry arising from the charge separation is almost planar. In contrast, for $\Lambda_s \ll \mu_e^{-1/2}$, the electron sheath becomes thicker than the ion sphere, i.e., $\Delta\xi_f > \xi_f$, and the ions are subject to the self-potential field caused by the whole sphere as in the case of a Coulomb explosion. The geometrical effect is then spherical.

In Fig. 4 strong dependence of the curves on μ_e is observed for $\Lambda_s \ll \mu_e^{-1/2}$, in which the maximum ion energy
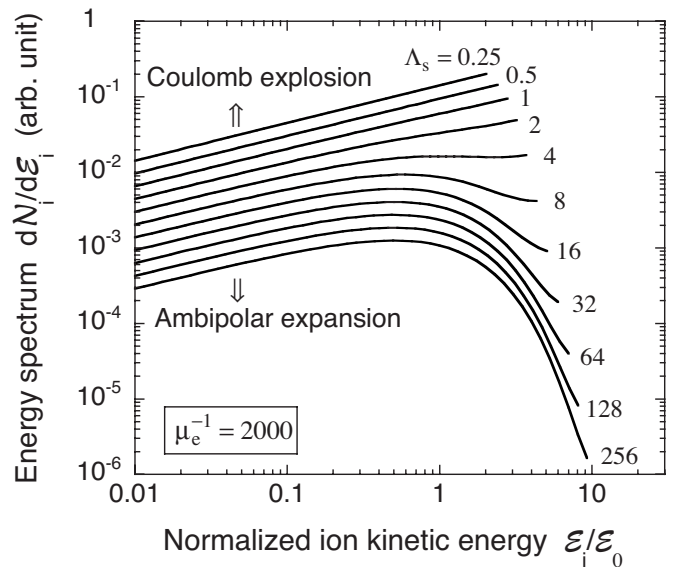
$\mathcal{E}_{i,\max}$ seemingly increases with decreasing μ_e at a fixed value of Λ_s. However this might lead readers to misunderstand the underlying physical picture such that the maximum ion energy of a Coulomb explosion, for example, would diverge to infinity as $\mu_e \to 0$. It is of course not the case, because the electron density profile will be stretched with decreasing μ_e [see Eq. (10)], and then the values of n_{e0} and thus Λ_s are correspondingly reduced [compare Eqs. (6) and (8)] under a finite amount of plasma; quantitatively this can be rephrased such that the three branch-off curves in Fig. 4 are just translation images with each other along the Λ_s-axis by a factor of $\mu_e^{3/4}$ as can be confirmed with the first formula of Eq. (18). The somewhat confusing physical picture for $\Lambda_s \ll \mu_e^{-1/2}$ mentioned above will be described in a simple manner in Sec. III in terms of the actual ion sphere size R_{u0} instead of the electron density scale R_0, or equivalently in terms of another dimensionless parameter Λ_u instead of Λ_s. As a matter of fact, the seeming μ_e-effect disappear on the $\mathcal{E}_{i,\max} - \Lambda_u$ plane (see Fig. 9 below), and the branch-off curves for $\Lambda_s \ll \mu_e^{-1/2}$ coalesce into a single curve [also see Eqs. (29) and (31) below].

The second important output of the self-similar solution is the energy spectrum of the ion kinetic energy. In view of Eq. (5), the distribution of ions $\mathcal{N}_i$ over their energy $\mathcal{E}_i = \mathcal{E}_0\xi^2$ at $t \to \infty$ is a simple image,

$$\frac{d\mathcal{N}_i}{d\mathcal{E}_i} = \frac{A}{\mathcal{E}_0}\left(\frac{\mathcal{E}_i}{\mathcal{E}_0}\right)^{\nu/2-1}[\exp(-\mathcal{E}_i/\mathcal{E}_0) + 2\nu\Lambda_s^{-2}], \quad 0 \leq \mathcal{E}_i \leq \mathcal{E}_{i,\max},$$

$$(21)$$

of the spatial distribution $N_i(\xi)$ applied to a finite energy interval $0 \leq \mathcal{E}_i \leq \mathcal{E}_{i,\max}$, where $A = (2\int_0^{\xi_f} N_i\xi^{\nu-1}d\xi)^{-1}$ is a constant, with which the total number of $\mathcal{N}_i$ is normalized to unity. Figure 5 shows the energy spectra ($\nu = 3$), Eq. (21), to demonstrate that its possible shapes range from a Coulomb-explosion spectrum in the limit of $\Lambda \to 0$, $d\mathcal{N}_i/d\mathcal{E}_i \propto \sqrt{\mathcal{E}_i/\mathcal{E}_0}$,

to the ambipolar expansion type[36] characterized by a Maxwellian exponent in the limit of $\Lambda_s \to \infty$, $d\mathcal{N}_i/d\mathcal{E}_i \propto \sqrt{\mathcal{E}_i/\mathcal{E}_0} \exp(-\mathcal{E}_i/\mathcal{E}_0)$. The spectrum for planar ($\nu=1$) mass-limited plasma has the form[10] $d\mathcal{N}_i/d\mathcal{E}_i \propto \exp(-\mathcal{E}_i/\mathcal{E}_0)/\sqrt{\mathcal{E}_i/\mathcal{E}_0}$. The limit $\Lambda_s \to \infty$ corresponds to quasineutral hydrodynamics, and our solution in this limit does indeed approach the corresponding self-similar solution of fluid dynamics. Good agreements in the energy spectrum between the self-similar solution, Eq. (21), and experiments are found in Ref. 10 in the limit $\Lambda_s \to \infty$. One should note however that our self-similar solution describes plasma expansion still in an approximate manner. In the opposite limit of $\Lambda_s \to 0$, when the ion density $N_i \approx 2\nu/\Lambda_s^2 \gg 1$ greatly exceeds the electron density $N_e \lesssim 1$, our solution describes the Coulomb explosion of a uniform bare ion sphere (or a cylinder or a slab) that has suddenly been deprived of all its electrons. A remarkable fact is that, as $\Lambda_s \to 0$, the modeled profiles for the velocity and the electric field are not only asymptotic for $t \to \infty$, but exact for all $t \geq 0$ in the particular case of a uniform initial density profile. It should be also noted that otherwise such characteristics of a Coulomb explosion as the energy spectrum, the temporal ion density, and the maximum ion energy depend on the initial density profile.[35]

III. APPLICATION OF THE SOLUTION TO NANOCLUSTER EXPLOSIONS

A. *N*-body particle simulation

Now consider a more practical case, where a droplet (or nanocluster) plasma with initial radius R_{u0} has uniform density profiles for both the ions and the electrons ($Zn_i=n_e=n_{u0}$) as shown in Fig. 1(a). This uniform profile decays as the plasma expands into vacuum. As a result, the profiles are expected to asymptotically approach those of the self-similar solution. In the following simulation, the ions are assumed to be cold at $t=0$, while the electrons are heated uniformly to a temperature T_{e0} with a Maxwellian distribution. In Sec. II, we saw that the self-similar dynamics of the expanding plasma are uniquely characterized by the external parameter Λ_s. What is the corresponding value of $\Lambda_s = \Lambda_s(R_{u0}, n_{u0}, T_{e0})$ describing a droplet plasma expansion in terms of the self-similar solution? We first find the parametric relation between a droplet plasma and the self-similar plasma. We then predict the maximum ion energy and the electron-to-ion energy transfer efficiency of a droplet plasma.

These analytical predictions are next tested by *N*-body charged particle simulations,[28,29] in which all the particle-to-particle Coulomb forces are computed exactly including a core-exclusion treatment to avoid numerical divergences.[29] The *N*-body simulation is the most suitable numerical approach to treat the parametric domain $\Lambda_s \ll \mu_e^{-1/2}$ (corresponding to a Coulomb explosion). In this domain, the plasma scale becomes less than or equal to the Debye length. In other words, each pair of ions in the ion sphere are influenced by their Coulomb potential, and a general particle-in-cell (PIC) simulation is inapplicable. Furthermore the *N*-body simulation will describe the dynamics of a system when its size and the ratio of the Coulomb energy to the

kinetic energy drastically changes in time. Note that $\mu_e^{-1}=100$ is employed in the present simulation to save CPU time and that $Z=1$ is used for simplicity. We have adopted the relativistic version of the Newton equations of motion, similar to the nonrelativistic molecular dynamics simulations used for studying microwave heating of (salty) water and ice.[29] The electrostatic and Lennard-Jones forces are calculated for pairs of atoms. The equations of motion are

$$\frac{d\mathbf{p}_i}{dt} = -\nabla\left\{ \sum_j \frac{q_i q_j}{r_{ij}} + 48\epsilon_{ij}\left[\left(\frac{\sigma}{r_{ij}}\right)^{12} - \left(\frac{\sigma}{r_{ij}}\right)^6\right] \right\}, \quad (22)$$

$$\frac{d\mathbf{r}_i}{dt} = \mathbf{v}_i, \quad \mathbf{p}_i = m_{i0}\mathbf{v}_i/\sqrt{1-(\mathbf{v}_i/c)^2}, \quad (23)$$

where $\mathbf{r}_i$, $\mathbf{v}_i$, and $\mathbf{p}_i$ are the position, velocity, and momentum of the ith atom, respectively; m_{i0} and q_i are its rest mass and charge, respectively, and $r_{ij}=|\mathbf{r}_i-\mathbf{r}_j|$ is the distance between the ith and jth atoms. The second term in the square bracket of the first equation serves to avoid the divergence in the Coulomb force ($r_{ij} \to 0$) by prohibiting overlap of the atoms, where σ is the sum of the radii of the two atoms and ϵ_{ij} is the Lennard-Jones energy. The Lennard-Jones potential is truncated at $2^{1/6}\sigma$ to limit its influence at short ranges. The ion and an electron radii are $\sigma_i=0.13$ nm and $\sigma_e=0.029$ nm, respectively. The time step for integration is 0.0165 fs. In the following simulations, the total number of electrons is fixed at $N_T \simeq 4200$, which is the number of electrons number contained in an actual hydrogen cluster for ($n_{e0}=10^{21}$ cm^{-3}, $R_{u0}=10$ nm) or ($n_{e0}=10^{23}$ cm^{-3}, $R_{u0}=2.15$ nm). Figure 6 shows a resulting *N*-body particle simulation as a series of snapshots of the particle positions in an exploding nanocluster composed of 4162 electrons with charge $q=-e$ and mass $m=m_e$, 3562 background ions with $q=+e$ and $m=100m_e$, and 150 impurity ions with $q=+4e$ and $m=100m_e$. The other parameters are $R_{u0}=2.15$ nm, $n_{u0}=10^{23}$ cm^{-3}, and $T_{e0}=4500$ eV. The left and right columns in Fig. 6 correspond to the electrons and the two-species ions, respectively. After the charge separation is built up due to the outburst of the electrons, the ions are accelerated outward by the strong sheath electrostatic field, resulting from the charge separation. The purpose of homogeneous doping of the impurity ions is to generate a quasimonoenergetic ion spectrum. In this case, the impurity ions are indeed accelerated quasimonoenergetically at around four times the maximum background ion energy, as will be discussed in more detail in Sec. IV.

How many particles are necessary to obtain a physically meaningful result with the *N*-body simulation? This question can be rephrased in the context of our problem as: What is the applicable range of Λ_u and Λ_s? Note that $\Lambda_u \approx \Lambda_s$ for $\Lambda_s \gg \mu_e^{-1/2}$ (see Fig. 7). We argue this problem in terms of the fraction of ions accelerated to maximum energies $\mathcal{E}_i \simeq \mathcal{E}_{i,\max}$, given in the form $\Delta\mathcal{N}_{i,f} \approx \mathcal{E}_{i,\max}(d\mathcal{N}_i/d\mathcal{E}_i)_{\mathcal{E}=\mathcal{E}_{i,\max}} = 2\xi_f^{\nu+2}/\Gamma(\nu/2)\Lambda_s^2$.[12] A fitted formula, $\Delta\mathcal{N}_{i,f} \approx (0.1\Lambda_s)^{-1.5}$, is numerically obtained for $30 < \Lambda_s < 3000$ when $\nu=3$. If the number of accelerated ions contained in the highest energy group is required to be more than 10, this condition is given by $N_T\Delta\mathcal{N}_{i,f} > 10$. The criteria is then reduced to $N_T > 0.3\Lambda_s^{1.5}$ using the above fitting formula. Thus the present
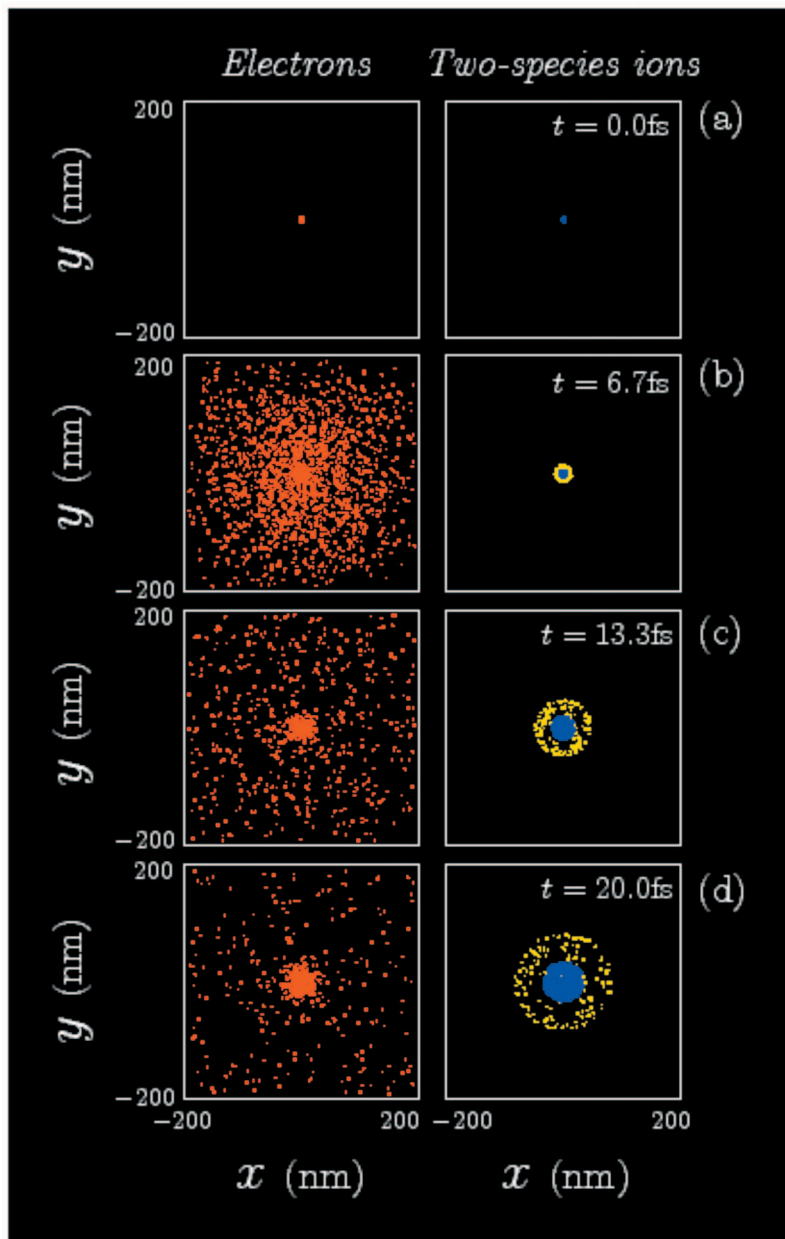
FIG. 6. (Color) Temporal evolution of the particle positions obtained by N-body simulation; the exploding nanocluster is composed of background ions ($Z=1$, blue dots) and impurity ions ($Z=4$, yellow dots) with the same mass ratio $m_i=m_p=100m_e$. Other parameters are $R_{u0}=2.15$ nm, $n_{u0}=10^{23}$ cm^{-3}, $T_{e0}=4500$ eV. The charge separation is established after the outburst of the electrons in (b). The ions are set into radial acceleration being driven by the strong sheath electrostatic field.

N-body simulation with $N_T \simeq 4200$ is expected to give us physically meaningful results for plasma expansions with $\Lambda_s < \mathcal{O}(10^2 - 10^3)$. This contrasts with PIC simulations, which is generally applicable for $\Lambda_s > \mathcal{O}(10 - 10^2)$.

B. Parametric relation between the solution and nanoclusters

In the following, we mainly focus consideration on a spherical geometry ($\nu=3$). We introduce two dimensionless parameters to characterize an initially uniform droplet plasma: The plasma size Λ_u [compare Eq. (8)] and the ion front position ξ_u,

$$\Lambda_u = R_{u0}\left(\frac{4\pi e^2 n_{u0}}{T_{e0}}\right)^{1/2}, \quad \xi_u = \frac{R_{u0}}{R_0}. \tag{24}$$

Note the difference between R_{u0} and $R_0 = R(0)$, where $R(t)$ is the temporal scale length defining the Maxwellian density

profile of the self-similar solution, Eqs. (5) and (13). We assume here that the electrons in the uniform plasma ($Zn_i = n_e = n_{u0}$) at $t=0$ are allowed to suddenly expand and that as a result they are quickly redistributed according to the spatial profile of the self-similar solution with $Zn_i \neq n_e = n_{e0}$ at $r=t=0$. Then the initial electron density ratio at the center, n_{u0}/n_{e0}, is given by Eqs. (13) and (14) as

$$\frac{n_{u0}}{n_{e0}} = \left.\frac{N_i}{N_e}\right|_{\xi=0} = 1 + \frac{6}{\Lambda_s^2}. \tag{25}$$

With the help of Eqs. (8), (13), (14), (24), and (25), Λ_u and ξ_u are related to Λ_s in the form

$$\Lambda_u = \xi_u\sqrt{\Lambda_s^2 + 6}. \tag{26}$$

As already mentioned, the density profiles are deformed from the initial ones in Fig. 1(a) to approach those in Fig. 1(b) and the ion energy spectrum becomes comparable to the
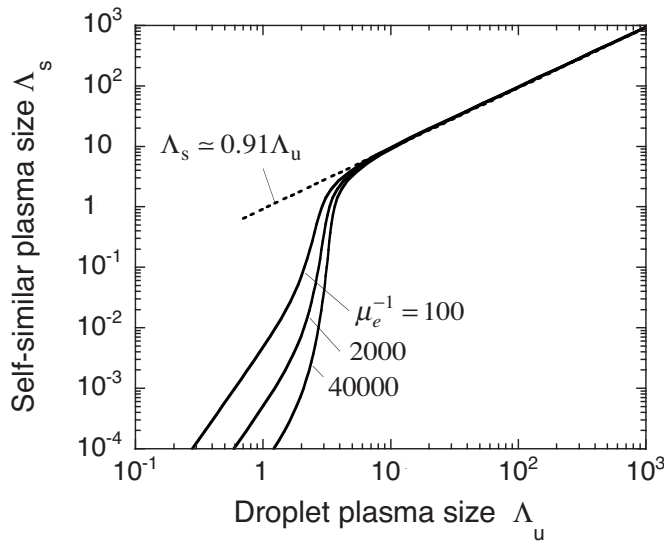
FIG. 7. Self-similar plasma size Λ_s vs droplet plasma size Λ_u for three different values, $\mu_e^{-1}=100$, 2 000 ($\approx$proton), and 40 000 ($\approx$sodium ion). The dashed line is fitted to the numerical results for $\Lambda_u \gg 10$.
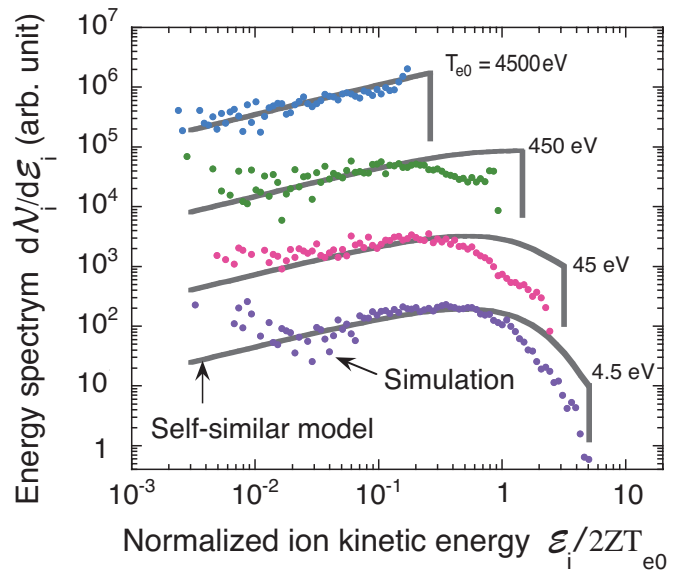

FIG. 8. (Color) Comparison of the ion energy spectrum for the self-similar model and the simulations; the parameters are $\mu_e^{-1}=100$, $Z=1$, $n_{u0}=10^{23}$ cm^{-3}, and $R_{u0}=2.15$ nm.

self-similar prediction of Eq. (21), as will be confirmed by the simulation results. Using Eqs. (8), (13), (14), (24), and (25), the ion mass conservation relation between the self-similar plasma and the droplet plasma reads

$$\int_0^{\xi_f} 4\pi\xi^2[\exp(-\xi^2)+6\Lambda_s^{-2}]d\xi = \frac{4}{3}\pi\xi_u^3(1+6\Lambda_s^{-2}). \quad (27)$$

Equations (26) and (27) give Λ_s and ξ_u as a function of Λ_u in terms of the initial parameters R_{u0}, T_{e0}, and n_{u0}. In particular, Eq. (27) gives an analytical expression for ξ_u in the two limiting regions, $\Lambda_s \ll \mu_e^{-1/2}$ and $\Lambda_s \gg \mu_e^{-1/2}$,

$$\xi_u = \begin{cases} \xi_f, & \Lambda_s \ll \mu_e^{-1/2}, \\ (3\sqrt{\pi}/4)^{1/3}, & \Lambda_s \gg \mu_e^{-1/2}. \end{cases} \quad (28)$$

Figure 7 shows Λ_s plotted against Λ_u for the three different values, $\mu_e^{-1}=100$, 2 000, and 40 000. The physical reasons for the bifurcation and the strong dependence on μ_e for $\Lambda_s \ll \mu_e^{-1/2}$ is the same as that given for Fig. 4. In contrast, for $\Lambda_s \gg \mu_e^{-1/2}$, one obtains from Eqs. (26) and (28) the proportionality $\Lambda_s \approx 0.91\Lambda_u$ regardless of the value of μ_e, which is depicted as the dotted line in Fig. 7.

C. Energy spectrum and maximum ion energy

Figure 8 compares the ion energy spectra comparing for the self-similar solution and the simulations. The fixed parameters are $Z=1$, $n_{u0}=10^{23}$ cm^{-3}, and $R_{u0}=2.15$ nm, while the initial temperature is varied over the range $T_{e0}=4.5-4500$ eV, with corresponding values of $\Lambda_u=1.4-43$. The vertical positions of the simulation data and the model curves were adjusted to best fit each other. Meanwhile the ion kinetic energy on the horizontal axis is normalized by $\mathcal{E}_0=2ZT_{e0}$ for both the self-similar model and the simulations. As a whole, the simulation results agree well with the model. The differences between them, particularly at higher energies, can be attributed to those of the initial profiles (see Fig. 1) and to thermodynamics. Regarding the latter, in the

expanding periphery the plasma cannot actually remain isothermal (as is assumed in the self-similar analysis), because the number of electron-electron collisions declines. That reduces the energy supply from the central region, resulting in weaker electric field and thus in decreased acceleration of the periphery ions at high energies.

The maximum ion kinetic energy $\mathcal{E}_{i,\max}/\mathcal{E}_0$ is a function of only Λ_u. Figure 9 compares $\mathcal{E}_{i,\max}/\mathcal{E}_0$ for the self-similar model and the simulation results. Using Eqs. (16), (26), and (28), $\mathcal{E}_{i,\max}/\mathcal{E}_0$ is analytically given in the two limiting regions, $\Lambda_u \ll 10$ and $\Lambda_u \gg 10$, as
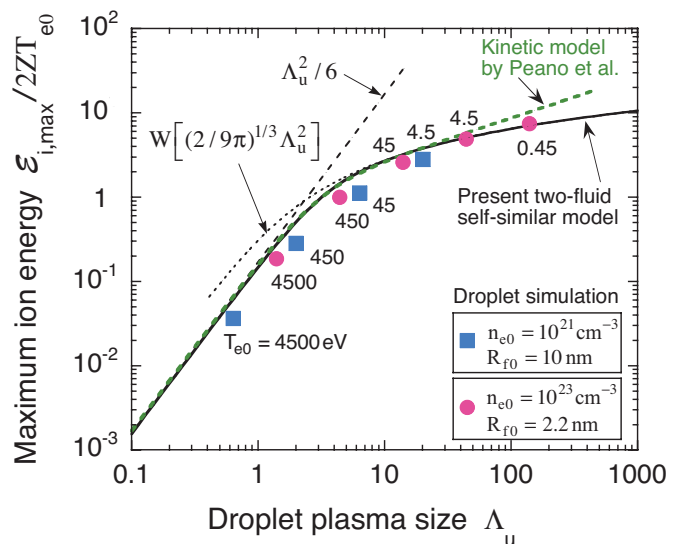

FIG. 9. (Color) Comparison of the maximum ion kinetic energy for the model (solid curve) and the simulations. The dashed curves plot the analytical solution in the two limits $\Lambda_u \rightarrow 0$ and $\Lambda_u \rightarrow \infty$. The solid curve represents the analytical fitting formula, Eq. (30), while the dashed curve is a fit to the kinetic model of Peano et al. (Ref. 14).

$$\frac{\mathcal{E}_{i,max}}{\mathcal{E}_0} = \begin{cases} \Lambda_u^2/6, & \Lambda_u \ll 10, \\ W[(2/9\pi)^{1/3}\Lambda_u^2], & \Lambda_u \gg 10, \end{cases} \quad (29)$$

which are depicted in Fig. 9 by the short- and long-dashed lines. The strong dependence of $\mathcal{E}_{i,max}(\Lambda_s, \mu_e)$ on μ_e for $\Lambda_s \ll \mu_e^{-1/2}$ observed in Fig. 4 disappears in the expression in Eq. (29). Note that no appreciable difference in the ion energy spectrum and the maximum ion energy can be found from a few test simulations when employing $\mu_e = 400$ instead of $\mu_e = 100$ for $\Lambda_u \approx 1$, 10, and 100. The two asymptotic analytical curves in Eq. (29) are combined to yield a fitting curve that applies to the whole domain, $0 < \Lambda_u < \infty$, as depicted by the solid curve in Fig. 9,

$$\frac{\mathcal{E}_{i,max}}{\mathcal{E}_0} \approx \left(\frac{1}{(\Lambda_u^2/6)^2} + \frac{1}{\{W[(2/9\pi)^{1/3}\Lambda_u^2]\}^2} \right)^{-1/2}, \quad 0 < \Lambda_u < \infty. \quad (30)$$

Recalling $\mathcal{E}_0 = 2ZT_{e0}$ for the instantaneous heating case and the definition of Λ_u [see Eq. (24)], the absolute value of $\mathcal{E}_{i,max}$ is explicitly given by

$$\mathcal{E}_{i,max} = \begin{cases} (4\pi/3)n_{u0}Ze^2R_{u0}^2, & \Lambda_u \ll 10, \\ 2ZT_{e0}W[(2/9\pi)^{1/3}\Lambda_u^2], & \Lambda_u \gg 10. \end{cases} \quad (31)$$

The first expression for $\Lambda_u \ll 10$ reproduces the maximum energy of the Coulomb explosion of a uniform bare ion sphere, and $\mathcal{E}_{i,max}$ does not depend on the electron temperature T_{e0} in this limit.

It is interesting to compare our results with those of Peano et al.[14] They also studied the same problem, namely, expansion of spherical plasmas composed of cold ions and hot electrons, using a novel kinetic model tested by PIC simulations. They proposed simple fitting formulae for their numerical results for the maximum ion kinetic energy in the form $\mathcal{E}_{i,max}/2ZT_{e0} = (\Lambda_u^2/6)\mathcal{F}_{1.43}(2.28\hat{T}_0^{3/4}) = (\Lambda_u^2/6)\mathcal{F}_{1.43}(2.28 \cdot 3^{3/4}\Lambda_u^{-3/2})$ with $\mathcal{F}_k(x) \equiv x/(1+x^k)^{1/k}$ and $\hat{T}_0 \equiv 3\lambda_D^2/R_0^2 = 3\Lambda_u^{-2}$ [compare Eq. (24) of the present paper and Eq. (5) in Ref. 14]. The dashed curve in Fig. 9 represents this fitting formula. Our results are in excellent accord with it.

D. Electron-to-ion energy transfer efficiency

Next we evaluate another important quantity, the fraction of the initial thermal energy of the electrons that is converted into kinetic energy of the ions at $t \to \infty$. Here we briefly demonstrate the energy accounting obtained from a numerical simulation of a nanocluster plasma expansion: Figure 10 shows the temporal behavior of the kinetic energy of the ions E_i, the kinetic energy of the electrons E_e, and the Coulomb potential energy E_C for the fixed parameters $Z=1$, $n_{u0} = 10^{23}$ cm^{-3}, $R_{u0} = 2.15$ nm, and $T_{e0} = 1400$ eV. Note that E_e is composed of the thermal energy and the radial translational kinetic energy; the former dominates E_e in the limit $t \to 0$ when $T = T_{e0}$, while the latter dominates in the limit $t \to \infty$ when $T = 0$. As is expected, substantial energy transfer occurs on a hydrodynamic time scale of $R_{u0}/c_{s0} \approx 6$ fs. As can be seen in Fig. 10, the electron energy is first converted into Coulomb potential energy to form the electron sheath,
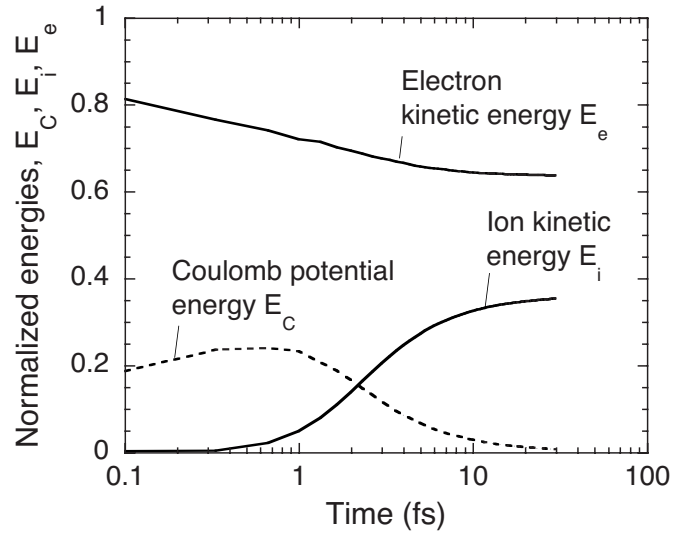

FIG. 10. Simulation results for the temporal evolution of the energies normalized by $E_e(0)$. The initial parameters are $Z=1$, $n_{u0}=10^{23}$ cm^{-3}, $R_{u0}=2.15$ nm, and $T_{e0}=1400$ eV.

and then the Coulomb energy is transferred to the ion kinetic energy, resulting in ion acceleration. In Fig. 10, the transferred energy from the electrons to the ions amounts to 35% at $t \to \infty$.

The self-similar model explicitly determines this transfer efficiency η_t as follows. The kinetic energy of the ions, $E_{ki} = \int \frac{1}{2}m_i n_i v_i^2 dV$ ($dV = 4\pi r^2 dr$), is calculated with the help of Eqs. (5)–(14) in the form

$$\frac{E_{ki}(t)}{E_0} = \frac{1}{3}\left\{ 1 - \left[\frac{R_0}{R(t)}\right]^{3(\gamma-1)} \right\} \int_0^{\xi_f} \xi^4[\exp(-\xi^2) + 6\Lambda_s^{-2}]d\xi, \quad (32)$$

where $E_0 = 8\pi R_0^3 n_{e0}T_{e0}/(\gamma-1)$. The thermal energy of the electrons, $E_{te} = (\gamma-1)^{-1}\int n_e T_e dV = (\gamma-1)^{-1}T_e\int Zn_i dV$ ($\int n_e dV = \int Zn_i dV$ is used), is

$$\frac{E_{te}(t)}{E_0} = \frac{1}{2}\left[\frac{R_0}{R(t)}\right]^{3(\gamma-1)}\int_0^{\xi_f} \xi^2[\exp(-\xi^2) + 6\Lambda_s^{-2}]d\xi. \quad (33)$$

Consequently the transfer efficiency is

$$\eta_t = \frac{E_{ki}(\infty)}{E_{te}(0)} = \frac{2\int_0^{\xi_f}\xi^4[\exp(-\xi^2) + 6\Lambda_s^{-2}]d\xi}{3\int_0^{\xi_f}\xi^2[\exp(-\xi^2) + 6\Lambda_s^{-2}]d\xi}, \quad (34)$$

where $\xi_f^2 = W(\Lambda_s^2/2)$ and Eqs. (26) and (27) were used to obtain ξ_f and Λ_s as a function of Λ_u. It should be noted that η_t is not influenced by the adiabatic index γ, as can be seen in Eq. (34). Figure 11 plots η_t versus Λ_u comparing the self-similar model (solid curve) of Eq. (34) with the simulation results. It is found that η_t dramatically changes in the region $1 \lesssim \Lambda_u \lesssim 10$. Our results for η_t agree with the fitting formula of Peano et al.,[14] graphed as the dashed curve in Fig. 11, where their fitting formula is given in a slightly modified form as $\eta_t = 1 - \mathcal{F}_{3.35}(1.86\Lambda_u^{-1})$, by redefining $\hat{T}_0 \equiv \Lambda_u^{-2}$ instead of $\hat{T}_0 \equiv 3\Lambda_u^{-2}$ [compare to Eq. (3) in Ref. 14].
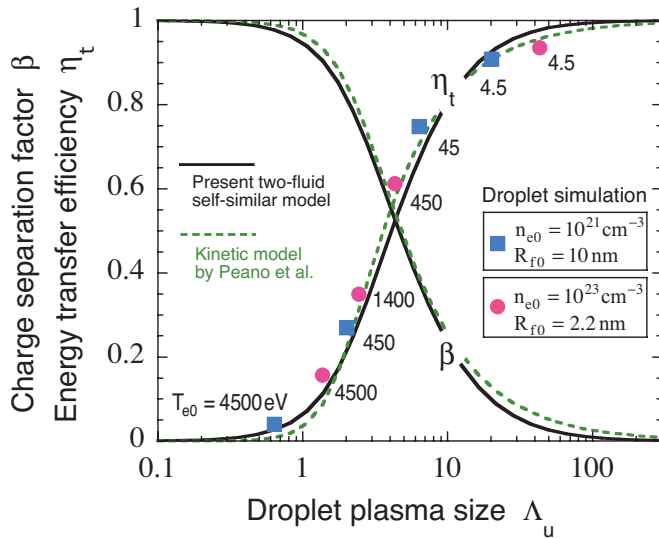
FIG. 11. (Color) Electron-to-ion energy transfer efficiency η_t and charge separation factor β as a function of the normalized initial radius of the nanoclusters Λ_u; $Z=1$ and $\nu=3$ are fixed. The symbols stand for the N-body particle simulations, while the solid and dashed curves denote our self-similar model and the kinetic model of Peano *et al.*, respectively.

FIG. 12. Final velocity ratio $v_{p\infty}/v_{f\infty}(=\xi_{p\infty}/\xi_f)$ vs self-similar plasma size Λ_s for different values of the normalized initial position of impurity ion ξ_{p0}/ξ_f.

E. Charge separation factor

The charge separation factor $\beta \equiv \int(N_i - N_e)dV / \int N_i dV$ (for the ion sphere), showing the extent to which electrons are "expelled" from the ion sphere, is also plotted in Fig. 11. With the help of Eqs. (13) and (14), β is computed by

$$\beta = 2\xi_f^3 \left[\Lambda_s^2 \int_0^{\xi_f} \xi^2 [\exp(-\xi^2) + 6\Lambda_s^{-2}]d\xi \right]^{-1}, \qquad (35)$$

where ξ_f and Λ_s are functions of Λ_u in the same manner as for η_t. In Fig. 11, the value of β obtained by our self-similar model is in good agreement with the fitting formula in Ref. 14, $\beta = \mathcal{F}_{2.60}(\sqrt{6/\exp(1)}\hat{T}_0^{1/2}) = \mathcal{F}_{2.60}(\sqrt{18/\exp(1)}\Lambda_u^{-1})$ with $\hat{T}_0 \equiv 3\Lambda_u^{-2}$ [see Eq. (2) in Ref. 14].

Figures 9 and 11 imply that our self-similar solution is a simple and robust analytical tool having good consistency with other kinetic approaches. Moreover, the results for the maximum ion energy $\mathcal{E}_{i,\max}$ and the energy transfer efficiency η_t suggest the following from an engineering point of view. When one wants to optimize the performance of a droplet plasma expansion in terms of $\mathcal{E}_{i,\max}$ and η_t, the dimensionless parameter Λ_u should be chosen so that $\Lambda_u \approx \mathcal{O}(1)$. This result could aid in the design of neutron sources using explosions of nanoparticles or atomic clusters,[37] for example.

IV. GENERATION OF QUASIMONOENERGETIC SPECTRUM

In our previous paper,[12] we discussed the test ion problem, where say protons are distributed on the surface of a high-Z spherical plasma and their resultant accelerations are calculated. In this section, we consider another extended problem, where impurity ions are distributed inside the plasma homogeneously. Here we use the term "impurity ions" instead of "test ions." If the impurity ions are substan-
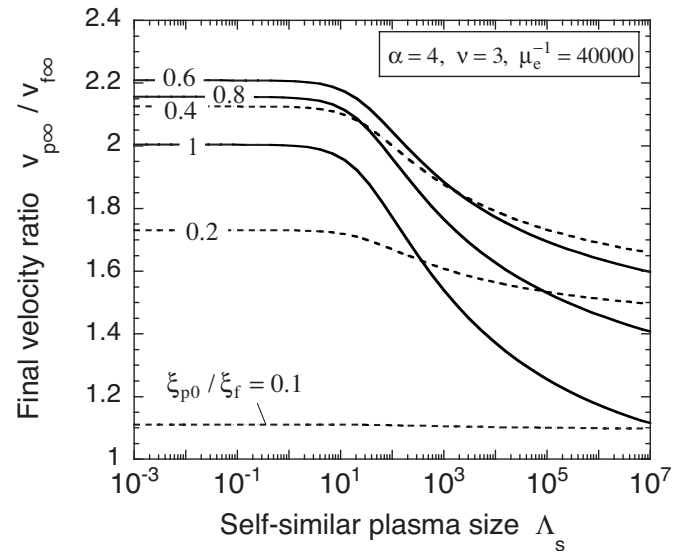
tially fewer in number than the background ions, the influence of the impurity ions on the electric field is expected to be negligibly small. In that case, the acceleration of the impurity ions can be deduced from the self-similar solution. We calculate the energy spectra of the impurity ions resulting from the plasma expansion into vacuum after the instantaneous heating.

Suppose that an impurity ion with mass m_p and electric charge $+Z_p e$ is initially at an arbitrary point in the bulk plasma described by our self-similar solution. As time elapses, its position $r_p(t)$ and velocity $v_p(t)$ increases. One can introduce the self-similar system size $R(t)$ as the independent parameter instead of time t, i.e., $r_p = r_p(R)$ and $v_p = v_p(R)$. Then the nonrelativistic dynamics of the impurity ion are governed by[12]

$$\frac{dr_p}{dR} = \frac{v_p}{2c_{s0}\sqrt{1 - R_0/R}}, \qquad (36)$$

$$\frac{dv_p}{dR} = -\frac{\alpha c_{s0}R_0}{2R^2\sqrt{1 - R_0/R}}\frac{d\Phi(\xi_p)}{d\xi}, \qquad (37)$$

where $\xi_p(R) = r_p(R)/R$, and

$$\alpha = \frac{Z_p/m_p}{Z/m_i} \qquad (38)$$

is a dimensionless parameter characterizing the charge-over-mass ratio of the impurity ion. Equations (36) and (37) are numerically integrated for $R(t) \geq R_0$ with initial conditions, $v_p(R_0) = 0$ and $r_p(R_0) = r_{p0}$, where r_{p0} is the initial position of the impurity ion satisfying $\xi_{p0} = r_{p0}/R_0 \leq \xi_f$.

The final velocity, $v_{p\infty} = v_p(\infty)$, of the impurity ion is a function of α and ξ_{p0}. Figure 12 plots the final velocity $v_{p\infty}$ normalized by the maximum ion velocity of the background ions $v_{f\infty}$ for different initial positions, ξ_{p0}/ξ_f, as a function of
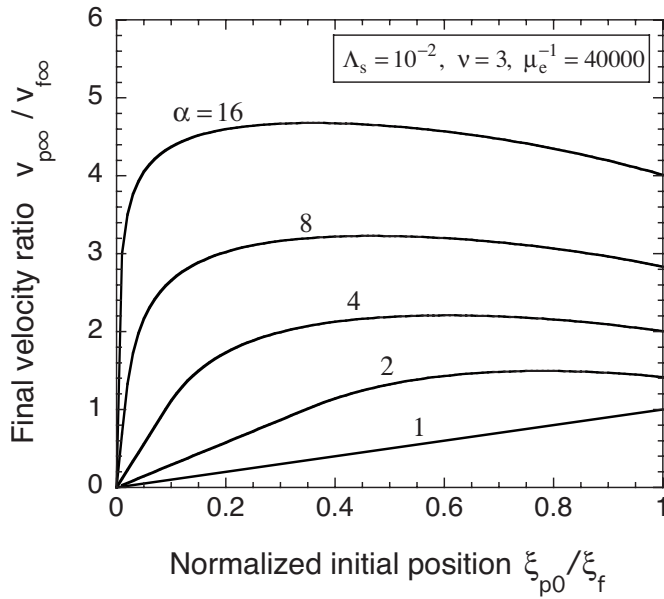
FIG. 13. Final velocity ratio $v_{p\infty}/v_{f\infty}(=\xi_{p\infty}/\xi_f)$ vs normalized initial position of impurity ion ξ_{p0}/ξ_f for different values of the charge-over-mass ratio α.
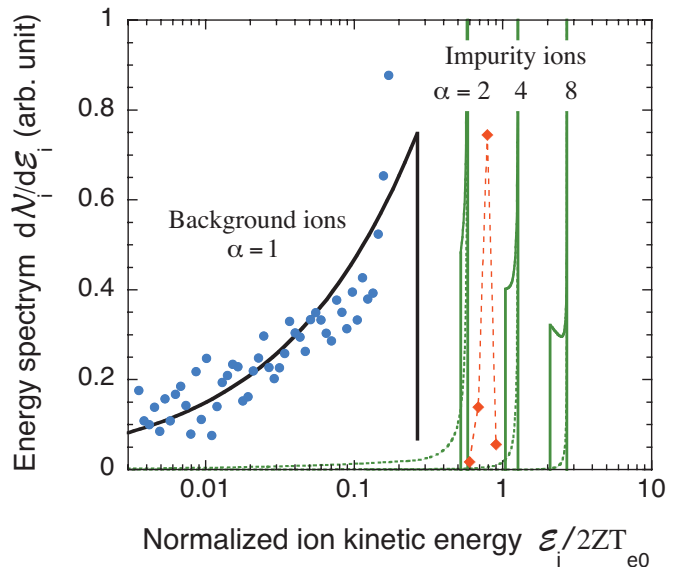

FIG. 14. (Color) Ion energy spectra for the background ions and the impurity ions comparing the self-similar model (curves) and the simulation (solid circles). Parameters for the simulation are $n_{u0}=10^{23}$ cm^{-3}, $R_{u0}=2.15$ nm, $T_{e0}=4500$ eV, and $\alpha=4$. (For two-dimensional plots, see Fig. 7.) The solid and dashed curves for the impurity ion spectra reveal the spatial origin of the ion emission corresponding to the outer region and the inner region of the ion sphere, respectively.

the self-similar plasma size Λ_s, where $\alpha=4$ and $\mu_e^{-1}=40\,000$ are fixed. According to Eq. (5), the velocity ratio equals the ratio of the self-similar coordinate ξ for an impurity ion and a background ion, i.e., $v_{p\infty}/v_{f\infty}=\xi_{p\infty}/\xi_{f\infty}$. One might have expected impurity ions on the plasma surface with $\xi_{p0}/\xi_f=1$ to attain the highest velocity, because they "feel" the highest electric field according to Figs. 2 and 3. However this conjecture is wrong, because all the impurity ions travel through the background ions and consequently increase their Lagrangian coordinates $\xi_p(t)$. What matters is the integrated work done by the electrostatic field on an ion $\int ZeE(r,t)dr$. As can be seen from Fig. 12, the highest value of $v_{p\infty}/v_{f\infty}$ is obtained for $\xi_{p0}/\xi_f\approx0.6$ if $\alpha=4$ and $\Lambda_s\lesssim100$.

Figure 13 shows $v_{p\infty}/v_{f\infty}$ as a function of ξ_{p0}/ξ_f with different values of α between 1 and 16, where $\Lambda_s=10^{-2}$ and $\mu_e^{-1}=40\,000$. The case of $\alpha=1$ corresponds to the background ions themselves, and therefore the line for $\alpha=1$ yields $v_{p\infty}/v_{f\infty}=\xi_{p\infty}/\xi_f=\xi_{p0}/\xi_f$. Also, an impurity ion located at the center keeps its position at all times. Furthermore $v_{p\infty}/v_{f\infty}\rightarrow\sqrt{\alpha}$ as $\xi_{p0}/\xi_f\rightarrow1$ for $\Lambda_s\lesssim\mu_e^{-1/2}$ (compare Fig. 12), because the ion acceleration is close to that for Coulomb explosions in the limit $\Lambda_s\rightarrow0$, where the maximum ion energy balances the initial Coulomb potential energy, i.e., $\frac{1}{2}m_p v_{p\infty}^2=Q_0 Z_p e/R_{u0}$ and thus $v_{p\infty}\propto\sqrt{Z_p/m_p}$, where Q_0 is the total ion sphere charge. A crucial implication in Fig. 13 is that a peak value of $v_{p\infty}/v_{f\infty}$ is achieved by specific impurity ions with their initial position $\xi_{p0}=\xi_{p0,\max}$, and that the curves of $v_{p\infty}/v_{f\infty}$ level off as can be seen in Fig. 13, becoming quasimonoenergetic. The flat shape is attributed to the finite-mass plasma in a spherical geometry. In the limits $\alpha\rightarrow\infty$ and $\Lambda_u\rightarrow0$, the achievable maximum kinetic energy of an impurity ion with its initial position ξ_{p0} is given in the simple form

$$\mathcal{E}_{p,\max}=\frac{3-(\xi_{p0}/\xi_f)^2}{2}\frac{Q_0 Z_p e}{R_{u0}}. \tag{39}$$

This relation is further reduced by comparing $\mathcal{E}_{p,\max}$ with $\mathcal{E}_{i,\max}$ to give

$$\frac{Z_p}{Z}\leqslant\frac{\mathcal{E}_{p,\max}}{\mathcal{E}_{i,\max}}\leqslant\frac{3Z_p}{2Z}, \tag{40}$$

namely, the ratio of the maximum kinetic energies does not explicitly depend on α but is a function of only the ratio of the ion charges.

The quasimonoenergetic feature can be more easily observed when the curves in Fig. 13 are transformed into energy spectra $d\mathcal{N}_i/d\mathcal{E}_i$. Figure 14 shows energy spectra for the background ions ($Z=1$) and for the impurity ions ($Z_p=2$, 4, and 8) comparing the self-similar model (plotted as the curves) and the simulation (the circles). Fixed parameters for the simulation are $n_{u0}=10^{23}$ cm^{-3}, $R_{u0}=2.15$ nm, $T_{e0}=4500$ eV, and $Z_p=4$. The ion masses are fixed to be $m_i=m_p=100m_e$. The N-body simulation for this set of parameters was graphed in Fig. 7. These parameters correspond to $\Lambda_u=1.36$ and thus $\mathcal{E}_{i,\max}/\mathcal{E}_0=0.26$ for the background ions from Eq. (30). Then, as mentioned earlier, the energy spectrum of the background ions is close to $d\mathcal{N}_i/d\mathcal{E}_i\propto\sqrt{\mathcal{E}_i/\mathcal{E}_0}$ as in the Coulomb explosion of a uniform bare ion sphere. The number of impurity ions is only 150 (compared with 3600 for the background ions) in order to not degrade the self-consistent electric field. The vertical axis is in arbitrary units, so that the impurity ion spectra can be compared to the background ion spectra. Overall, the model prediction and the simulation results differ by a factor of about 1.5 along the horizontal axis. This discrepancy arises partly because the background electric field is not the same as the one predicted

by the self-similar solution due to the existence of the impurity ions. Nevertheless, a quasimonoenergetic spectrum is observed in the simulation with the expected energy enhancement, i.e., $\mathcal{E}_{p,\max}/\mathcal{E}_{i,\max} \simeq Z_p/Z = 4$. The solid and dashed lines for the impurity ion spectra reveal the spatial origin of the ion emission. The dashed curves for the impurity ions correspond to their initial values for $\xi_{p0} \lesssim \xi_{p0,\max}$. Meanwhile the solid curves correspond to their initial values for $\xi_{p0,\max} \lesssim \xi_{p0} \lesssim \xi_f$. The discrepancy between the self-similar model and a real system in the temporal evolution of the electric field is expected to become more substantial with a larger value of Λ_u, particularly at early times $t < R_{u0}/c_{s0}$. Recently another interesting idea has been proposed by Kumar and Pukhov.[23] They modified the analysis for the self-similar solution of Ref. [10] and introduced a new ingredient, namely, tailoring of laser pulses, to demonstrate the generation of quasimonoenergetic ion spectra.

V. SUMMARY

Nanocluster plasma expansion and the resultant ion acceleration have been studied both analytically and numerically. Key physical quantities such as the maximum kinetic energy $\mathcal{E}_{i,\max}$, the energy spectrum $d\mathcal{N}_i/d\mathcal{E}_i$, and the electron-to-ion energy transfer efficiency η_t have been expressed in simple formulae as a function of the dimensionless parameter $\Lambda_u = \Lambda_u(T_{e0}, R_{u0}, n_{u0})$. As a compromise between values of η_t and $\mathcal{E}_{i,\max}$ for the nanocluster explosions, Λ_u must be chosen to be of order unity.

We have generated quasimonoenergetic spectra using impurity ions that are homogeneously doped in a spherical pellet. The good agreements between the two quite different approaches, namely, the fluid description (our self-similar solution) and the kinetic descriptions (our *N*-body simulation and the work by Peano *et al.*), have revealed the underlying physical picture of the plasma expansion and the generation of the quasimonoenergetic spectrum. In a spherical system, an impurity ion undergoes an increasing and decreasing electric field inside and outside the ion sphere, respectively (Figs. 2 and 3). The final velocity profile of the impurity ions turns out to be rather flat with respect to their initial positions ξ_{p0} (Fig. 13). This acceleration mechanism and the resultant quasimonoenergetic spectrum are concluded to be peculiar to a spherical system.

[1] A. Pukhov, Z.-M. Sheng, and J. Meyer-ter-Vehn, Phys. Plasmas **6**, 2847 (1999).

[2] K. Krushelnick, E. C. Clark, M. Zepf, J. R. Davies, F. N. Beg, A. Machacek, M. I. K. Santala, M. Tatarakis, I. Watts, P. A. Norreys, and A. E. Dangor, Phys. Plasmas **7**, 2055 (2000).

[3] S. C. Wilks, A. B. Langdon, T. E. Cowan, M. Roth, M. Singh, S. Hatchett, M. H. Key, D. Pennington, A. MacKinnon, and R. A. Snavely, Phys. Plasmas **8**, 542 (2001).

[4] P. Mora, Phys. Rev. Lett. **90**, 185002 (2003).

[5] S. V. Bulanov, T. Zh. Esirkepov, J. Koga, T. Tajima, and D. Farina, Plasma Phys. Rep. **30**, 18 (2004).

[6] B. N. Breizman, A. V. Arefiev, and M. V. Fomyts'kyi, Phys. Plasmas **12**, 056706 (2005).

[7] V. Yu. Bychenkov and V. F. Kovalev, Quantum Electron. **35**, 1143 (2005).

[8] E. d'Humières, E. Lefebvre, L. Gremillet, and V. Malka, Phys. Plasmas **12**, 062704 (2005).

[9] J. Fuchs, Y. Sentoku, S. Karsch, J. Cobble, P. Audebert, A. Kemp, A. Nikroo, P. Antici, E. Brambrink, A. Blazevic, E. M. Campbell, J. C. Fernández, J.-C. Gauthier, M. Geissel, M. Hegelich, H. Pépin, H. Popescu, N. Renard-LeGalloudec, M. Roth, J. Schreiber, R. Stephen, and T. E. Cowan, Phys. Rev. Lett. **94**, 045004 (2005).

[10] M. Murakami, Y.-G. Kang, K. Nishihara, S. Fujioka, and H. Nishimura, Phys. Plasmas **12**, 062706 (2005).

[11] M. Passoni and M. Lontano, Laser Appl. **13**, 042102 (2006).

[12] M. Murakami and M. M. Basko, Phys. Plasmas **13**, 012105 (2006).

[13] J. Schreiber, F. Bell, F. Grüner, U. Schramm, M. Gessler, M. Schnürer, S. Ter-Avetisyan, B. M. Hegelich, J. Cobble, E. Brambrink, J. Fuchs, P. Audebert, and D. Habs, Phys. Rev. Lett. **97**, 045005 (2006).

[14] F. Peano, F. Peinetti, R. Mulas, G. Coppa, and L. O. Silva, Phys. Rev. Lett. **96**, 175002 (2006).

[15] T. Zh. Esirkepov, S. V. Bulanov, K. Nishihara, T. Tajima, F. Pegoraro, V. S. Khoroschkov, K. Mima, H. Daido, Y. Kato, Y. Kitagawa, K. Nagai, and S. Sakabe, Phys. Rev. Lett. **89**, 175003 (2002).

[16] V. Yu. Bychenkov, V. N. Novikov, D. Batani, V. T. Tikhonchuk, and S. G. Bochkarev, Phys. Plasmas **11**, 3242 (2004).

[17] A. J. Kemp and H. Ruhl, Phys. Plasmas **12**, 033105 (2005).

[18] V. T. Tikhonchuk, A. A. Andreev, S. G. Bochkarev, and V. Yu. Bychenkov, Plasma Phys. Controlled Fusion **47**, B869 (2005).

[19] B. M. Hegelich, B. J. Albright, J. Cobble, K. Flippo, S. Letzring, M. Paffett, H. Ruhl, J. Schreiber, R. K. Schulze, and J. C. Fernández, Nature (London) **439**, 441 (2006).

[20] I. Last and J. Jortner, Phys. Rev. A **71**, 063204 (2005).

[21] S. Ter-Avetisyan, M. Schürer, P. V. Nickles, M. Kalaschnikov, E. Risse, T. Sokollik, W. Sandner, A. Andreev, and V. Tikhonchuk, Phys. Rev. Lett. **96**, 145006 (2006).

[22] V. F. Kovalev, V. Yu. Bychenkov, and K. Mima, Phys. Plasmas **14**, 103110 (2007).

[23] N. Kumar and A. Pukhov, Phys. Plasmas **15**, 053103 (2008).

[24] A. P. L. Robinson, A. R. Bell, and R. J. Kingham, Phys. Rev. Lett. **96**, 035005 (2006).

[25] K. Flippo, B. M. Hegelich, B. J. Albright, L. Yin, D. C. Gautier, S. Letzring, M. Schollmeier, J. Schreiber, R. Schulze, and J. C. Fernández, Laser Part. Beams **25**, 3 (2007).

[26] C. Sack and H. Schamel, Phys. Rep. **156**, 311 (1987).

[27] L. D. Landau and E. M. Lifshitz, *Statistical Physics*, 2nd ed. (Pergamon, Oxford, 1968), Sec. 38.

[28] G. M. Petrov, J. Davis, A. L. Velikovich, P. Kepple, A. Dasgupta, and R. W. Clark, Phys. Plasmas **12**, 063103 (2005).

[29] M. Tanaka and M. Sato, J. Chem. Phys. **126**, 034509 (2007).

[30] L. I. Sedov, *Similarity and Dimensional Methods in Mechanics*, 10th ed. (CRC, Boca Raton, 1993).

[31] R. M. Corless, G. H. Gonnet, D. E. G. Hare, D. J. Jeffrey, and D. E. Knuth, Adv. Comput. Math. **5**, 329 (1996).

[32] K. Nishihara, H. Amitani, M. Murakami, S. V. Bulanov, and T. Zh. Esirkepov, Nucl. Instrum. Methods Phys. Res. A **A464**, 98 (2001).

[33] D. S. Dorozhkina and V. E. Semenov, Phys. Rev. Lett. **81**, 2691 (1998).

[34] V. F. Kovalev and V. Yu. Bychenkov, Phys. Rev. Lett. **90**, 185004 (2003).

[35] A. E. Kaplan, B. Y. Dubetsky, and P. L. Shkolnikov, Phys. Rev. Lett. **91**, 143401 (2003).

[36] S. J. Gitomer, R. D. Jones, F. Begay, A. W. Ehler, J. F. Kephart, and R. Kristal, Phys. Fluids **29**, 2679 (1986).

[37] T. Ditmire, J. Zweiback, V. P. Yanovsky, T. E. Cowan, G. Hays, and K. B. Wharton, Nature (London) **398**, 489 (1999).